Bull Volcanol (2008) 70:455–473
DOI 10.1007/s00445-007-0149-y

RESEARCH ARTICLE

Volatile-induced magma differentiation in the plumbing system of Mt. Etna volcano (Italy): evidence from glass in tephra of the 2001 eruption

Carmelo Ferlito · Marco Viccaro · Renato Cristofolini

Received: 17 February 2006 / Accepted: 17 May 2007 / Published online: 10 July 2007
© Springer-Verlag 2007

Abstract Mount Etna volcano was shaken during the summer 2001 by one of the most singular eruptive episodes of the last centuries. For about 3 weeks, several eruptive fractures developed, emitting lava flows and tephra that significantly modified the landscape of the southern flank of the volcano. This event stimulated the attention of the scientific community especially for the simultaneous emission of petrologically distinct magmas, recognized as coming from different segments of the plumbing system. A stratigraphically controlled sampling of tephra layers was performed at the most active vents of the eruption, in particular at the 2,100 m (CAL) and at the 2,550 m (LAG) scoria cones. Detailed scanning electron microscope and energy dispersive x-ray spectrometer (SEM-EDS) analyses performed on glasses found in tephra and comparison with lava whole rock compositions indicate an anomalous increase in Ti, Fe, P, and particularly of K and Cl in the upper layers of the LAG sequence. Mass balance and thermodynamic calculations have shown that this enrichment cannot be accounted for by "classical" differentiation processes, such as crystal fractionation and magma mixing. The analysis of petrological features of the magmas involved in the event, integrated with the volcanological evolution, has evidenced the role played by volatiles in controlling the magmatic evolution within the crustal portion of the plumbing system. Volatiles, constituted of H_2O, CO_2, and Cl-complexes, originated from a deeply seated magma body (DBM). Their upward migration occurred through a fracture network possibly developed by the seismic swarms during the period preceding the event. In the upper portion of the plumbing system, a shallower residing magma body (ABT) had chemical and physical conditions to receive migrating volatiles, which hence dissolved the mobilized elements producing the observed selective enrichment. This volatile-induced differentiation involved exclusively the lowest erupted portion of the ABT magma due to the low velocity of volatiles diffusion within a crystallizing magma body and/or to the short time between volatiles migration and the onset of the eruption. Furthermore, the increased amount of volatiles in this level of the chamber strongly affected the eruptive behavior. In fact, the emission of these products at the LAG vent, towards the end of the eruption, modified the eruptive style from classical strombolian to strongly explosive.

Keywords Mount Etna · 2001 eruption · Tephra, Residual glass · Alkali enrichment · Volatile-induced differentiation · Chlorine

Editorial responsibility: M. Clynne

C. Ferlito · M. Viccaro · R. Cristofolini (✉)
Dipartimento di Scienze Geologiche,
Università degli Studi di Catania,
Corso Italia 57,
95129 Catania, Italy
e-mail: rcristof@unict.it

Introduction

The role of volatiles in modifying the chemical composition of a geological system is considered as relevant especially in the evolution of plutonic complexes or metamorphic rocks. In particular, in igneous environments, a volatile-induced differentiation, that is a mass transfer of volatile components carrying mobile elements, produces profound chemical changes of the rocks which are often associated with ore deposits (Boudreau et al. 1986; Hedenquist and Lowenstern 1994 and references therein; Keppler and Wyllie 1990, 1991; MacDonald et al. 1973; Rae et al. 1996; Salvi and William-Jones 1996; Webster

1992, 1997; Wilkinson et al. 1996). Little is known on the behavior of volatiles at pressures and temperatures of the volcanic environment (Burnham 1979; Caroff et al. 1997; De Hoogh and Van Bergen 2000; Greenough et al. 1999) and, moreover, on the effects that fluids can exert on magmatic melts and on their "differentiation" (meaning in more general terms the diversification of magmas). Some authors have suggested the possible role of volatiles in the evolution particularly of peralkaline acid products (e.g., comendites; Bohrson and Reid 1997; Davies and MacDonald 1987; MacDonald et al. 1987; Taylor et al. 1981). However, only modest attention has been so far paid to the investigation of "volatile-induced differentiation" in the evolution of Etnean magmas. Since 1971, Etnean volcanics have been characterized by a progressive K, Rb, Cs, and $^{87}Sr/^{86}Sr$ increase associated with lower contents of other incompatible elements such as Th. Several authors have suggested different scenarios to explain the origin of such an enrichment: (1) selective contamination by sediments underlying the volcanic edifice (Joron and Treuil 1984; Clocchiatti et al. 1988; Condomines et al. 1995; Tonarini et al. 1995; Tanguy et al. 1997); (2) contribution of a fluid component possibly derived from the subducting Ionian slab (Schiano et al. 2001; Tonarini et al. 2001; Armienti et al. 2002); and (3) characters inherited by a chemically and isotopically heterogeneous mantle source (Armienti et al. 1989; Barbieri et al. 1993; Corsaro and Cristofolini 1996). In such a picture, the magmatic differentiation induced by volatiles in the plumbing system could represent a significant contribution to understand the evolution of Etnean magmas after 1971. The interest for investigating the volatile differentiation arose during the petrochemical study of the products of 2001 eruption.

The July–August 2001 eruption, which occurred on the southern flank of the volcano, is one of the most thoroughly investigated episodes of the last few decades. Considerable literature has described the many aspects of this complex eruption (Bonaccorso et al. 2004; Clocchiatti et al. 2004; Métrich et al. 2004; Monaco et al. 2005; Viccaro et al. 2006). One of its most intriguing features was the simultaneous activation of two independent fracture systems trending NNW-SSE (SE-PL = SE crater–Piano del Lago) and N-S (C–L = Calcarazzi–Laghetto; Monaco et al. 2005), which erupted trachybasaltic magmas with distinct compositional features (Fig. 1).

All previous work (Behncke and Neri 2003; Lanzafame et al. 2003; Clocchiatti et al. 2004; Métrich et al. 2004; Monaco et al. 2005; Corsaro et al. 2007; Viccaro et al. 2006) specifically indicates that the feeders of the C–L magma were unrelated to the main axial conduit system (i.e., eccentric). Viccaro et al. (2006) clarify the complex relationship between the magmas erupted from the C–L

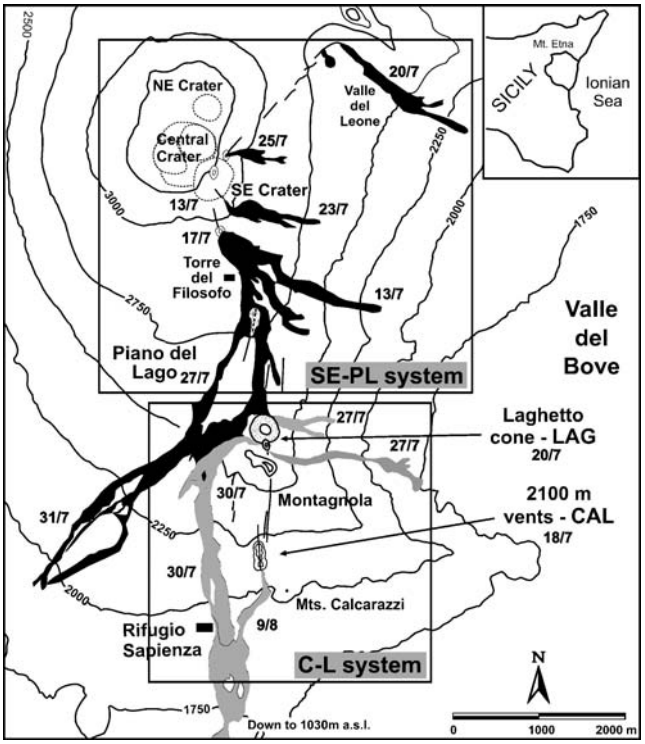

Fig. 1 Sketch map of the southern flank of Mount Etna volcano with the SE crater–Piano del Lago (*SE–PL*) and Calcarazzi–Laghetto (*C–L*) fracture systems, vents, and lava flows of the 2001 eruption. *Solid lines* represent visible eruptive and dry fissures, whereas *dashed lines* are fissures buried by lava flows. Lavas buried by ensuing flows are not shown on map. SE–PL lavas are shown in *black* and C–L ones in *light gray*. All dates refer to the onset of the relative eruptive episode. Further detailed maps and information are available at http://www.ct.ingv.it

system and their styles and times of eruption that displayed the occurrence of mixing. The process involved an amphibole-bearing trachybasalt (ABT in this work), residing at ~6 km (b.s.l.) erupted at the Calcarazzi vent (CAL) and a more basic and deeper end-member (DBM), which never reached the surface during the event. Products erupted towards the final phase of the eruption at the Laghetto vent (Fig. 1; LAG) showed a compositional variability attributed to the mixing of DBM and ABT.

This work focuses on the systematic sampling of tephra layers related to the explosive activity of the C–L system. Microanalyses on glasses found in tephra allow us to investigate classical differentiation processes such as crystal fractionation and fsmagma mixing. However, glass and bulk rock compositions can be successfully interpreted by means of mass balance and thermodynamic calculations only if the role of volatile components is considered in the differentiation of the products erupted at LAG. The magma differentiation brought about by volatile transfer has left a typical geochemical signature which is superimposed on the composition derived by magma mixing. The possibility of the volatile migration through different segments of the

feeding system is facilitated by the presence of fracture networks. Geophysical data support the hypothesis that volatiles were mostly transferred during the months preceding the onset of the eruption. Results presented here provide a contribution for the understanding of the complex dynamics presently acting on the plumbing system of Mount Etna, emphasizing the importance of volatile transfer in inducing differentiation of Etnean magmas.

Volcanological evolution of the 2001 eruption

The 2001 eruption is summarized here, the reports of INGV-Sezione di Catania (http://www.ct.ingv.it) give more detailed descriptions.

The eruption of July–August 2001 was preceded by two main seismic crises below the southern flank of Mt. Etna: one in January 2001, and the other, more significant with approximately 200 events, on April 20 (Bonaccorso et al. 2004). The hypocenters of this second swarm were located at depths between 5 and 10 km b.s.l., underneath the central-southern region of Mt. Etna. This hypocentral distribution constrains the main seismogenic fault plane along a NE-SW orientation (Bonaccorso et al. 2004). The opening of the eruptive fractures was immediately preceded by a seismic crisis with about 2,600 shallow earthquakes (Bonaccorso et al. 2002, 2004; Patanè et al. 2002; Billi et al. 2003; Lanzafame et al. 2003; Alparone et al. 2004). On July 13, the first lava fountain occurred at the SE crater, and in the following days, eruptive fissures, oriented NNW-SSE, progressed southwards to the Piano del Lago area (Fig. 1; SE-PL fracture system). Beginning July 15, the number of deeper earthquakes gradually vanished (Monaco et al. 2005). In the early morning of July 18, seismic activity ended and a new eruptive fissure, N-S oriented, opened near Mts. Calcarazzi at 2,100 m a.s.l. (CAL in Fig. 1).

Also on July 18, the N-S fractures progressed northwards for about 1.5 km and reached the Laghetto area at 2,550 m a.s.l. (LAG in Fig. 1), giving rise to the C–L fracture system. Meanwhile, the NNW-SSE-oriented fracturing progressed downslope along the Piano del Lago area and on July 20 intersected the N-S oriented fractures at the Laghetto area. Here, the extensional offset of the fractures doubled, creating a pit crater (Monaco et al. 2005). The initial activity had phreato-magmatic character, enhanced by the presence of a small and shallow aquifer until July 25, when lava fountains up to 500 m high indicated a change of the eruptive style and an increase in the juvenile component (Behncke and Neri 2003; Taddeucci et al. 2002; 2004). The explosive activity at LAG built a 60-m-high tephra cone in about 2 weeks (Calvari and Pinkerton 2004; Ferlito and Siewert 2006). Lava emission with a rather low output rate (2–6 m^3/sec) started from LAG on July 26, with short flows (400 m) directed south and longer flows on July 27 directed east into the Valle del Bove. In the evening of July 30, the lava output increased dramatically and gave rise to a large flow, 150 m wide at its front, that reached the Rifugio Sapienza area within a few hours (Ferlito and Siewert 2006). This was the climax of the July–August 2001 eruption, after which, no more lava was emitted by the LAG. In this final phase of the eruption, the explosive activity reached its peak, slowly decreasing until August 9. The entire eruption, recorded as one of the most explosive events of the century, produced an estimated volume of 25×10^6 m^3 of lava and 7×10^6 m^3 (DRE) of tephra (Behncke and Neri 2003; Lautze et al. 2004).

Field observations and sampling

Tephra layers

At the lowest end of the C–L fracture system (2,100 m a.s.l.), five scoria cones were built by the strombolian activity on a ~20° sloping flank. The upper cones are only few meters high, whereas the largest one is at the southern end of the fracture and it is about 30 m high, with a 30-m-wide crater. The effusive vent was located at the base of this cone. In the inner section of the crater, the uppermost levels are made up of loose tephra with grain sizes varying from ash to lapilli. It is possible to observe here coarsely and normally graded beds characterized by poor welding. The crater walls of the main cone were sampled from bottom to top. The finer-grained and less-welded fractions of three levels were collected (CAL 1–CAL 3) and sieved. The sample fractions finer than 2 mm were selected for further examinations.

At the highest end of the C–L fracture system (2,550 m a.s.l.), the Laghetto cone was built by the most violent strombolian activity observed during the entire eruption.

Tephra are mostly composed of 10–100 cm bombs and blocks, whereas meter-sized clasts are scarce as are lapilli and coarse ash. Bedding is rough and mainly exposed in the upper part of the sequence where it is normally graded. Coarse scoriaceous bombs and lapilli associated with scarce small bombs are prevailing in the lower levels of the sequence. In the upper half of the sequence, welded lapilli and ash grade upward from decimetric- to metric-thick beds. Samples were collected along the steep northeastern crater wall, where the most continuous vertical stratigraphic section is exposed and effects of fumarolic activity are absent (Fig. 2a, b). The finer-grained and less-welded fractions from seven levels were collected. Samples were labeled LAG 1 to LAG 7 from the

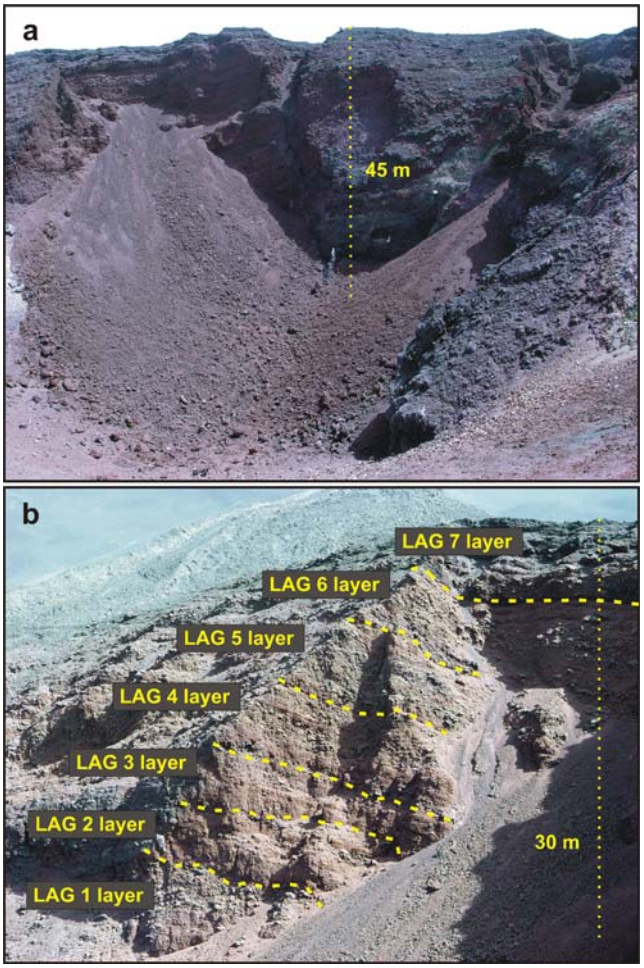

Fig. 2 **a** The eastern sector of the Laghetto crater inner wall; **b** Sequence of tephra layers sampled on the northern sector of the Laghetto crater inner wall

bottom to the top of the sequence and only clasts finer than 2 mm were chosen for analyses.

Lava flows

Lava flows were emitted from the C–L fracture system both at the CAL and LAG vents (Fig. 1). The flows from the CAL vent advanced southwards for 6.9 km to an elevation of 1,030 m. Lavas from the LAG vent flowed eastward, reaching the Valle del Bove floor (1,750 m a.s.l.), and southward to the Rifugio Sapienza area (ca. 1,950 m a.s.l.). Samples were collected during and immediately after the eruption from flow units belonging to all eruptive vents. Seventeen lava specimens of the C–L system have been collected: five of them, sampled at the lowermost front of the active flow on July 18, represent the first emitted lavas (CAL); the other twelve were collected at the base of the Laghetto cone (LAG) during the intermediate (26/7–28/7) and later stages (29/7–30/7) of the eruption, and they represent approximately members equivalent to the LAG 3 and LAG 7 tephra layers, respectively.

Features of erupted products

Petrography and chemistry of residual glass

CAL 1–3 tephra samples are very similar. Those selected for analyses are vitrophyric with euhedral phenocrysts of augite, plagioclase, and scarce Ti-magnetite and olivine. No amphibole phenocrysts have been found among the selected CAL 1–3 grains. Microlites are mostly plagioclase with subordinate augite and very scarce olivine and Ti-magnetite. In these layers, phenocrysts and microlites constitute about 25–30 vol.%. The vesicle volume in the samples CAL 1–3 is <50%, and the most abundant glass type is sideromelane. The scarcity of tachylytic glass indicates that the melt was quenched and significant amounts of Ti-magnetite could not nucleate (Fig. 3a).

In all the LAG samples, the vesicle volume is higher than in CAL ones (>50 vol.%), in accord with a higher level of explosiveness at LAG. The glass color changes from dark brown (LAG 1) to orange-brown (LAG 4) upward in the sequence due to decreasing alteration (Fig. 3b). In these lower levels, phenocrysts and microlites, mostly of plagioclase, with subordinate augite, olivine, and Ti-magnetite, constitute about 20–25 vol.%. Phenocrysts and microlites contents (15–20 vol.%) of the same phases decrease higher in the sequence (samples from LAG 5 to LAG 7). Also, among the selected LAG 1–7 tephra, no amphibole phenocrysts have been found. In LAG 5–7 beds, glass is limpid and clear showing that quenching was fast and efficient enough to prevent Ti-magnetite nucleation (Fig. 3c).

Samples, least affected by fumarole action, were selected for chemical analysis from three different levels (namely, CAL 1, LAG 3, and LAG 7), as representative, respectively, of the early, intermediate, and final eruptive phases of the C–L system.

Major element compositions of sideromelane were obtained at INGV (Sezione di Catania, Italy) by means of a LEO-1430 Scanning Electron Microscope equipped with an Oxford EDS microanalytical system at 20 kV acceleration voltage and 1,200 nA beam current. VG2 standard basaltic glass (Jarosewich et al. 1980) was used as an analytical standard. The accuracy is ~0.5% for abundances >15 wt%, ~1% for abundances around 5 wt%, and ~20% for abundances around 0.5 wt%. The precision is better than 1% for SiO_2, Al_2O_3, FeO, MgO, and CaO and better than 3% for TiO_2, MnO, Na_2O, K_2O, and P_2O_5. The CAL 1 and LAG 3 glasses are basaltic-trachyandesites in composition, whereas the LAG 7 glass is phono-tephritic (Table 1; Le Maitre 2002). All data compare well with scanning electron microscope and energy dispersive x-ray spectrometer (SEM-EDS) analyses for glasses from tephra layers of the Laghetto cone reported elsewhere (Taddeucci et al. 2004), confirming the quality of the analytical results.

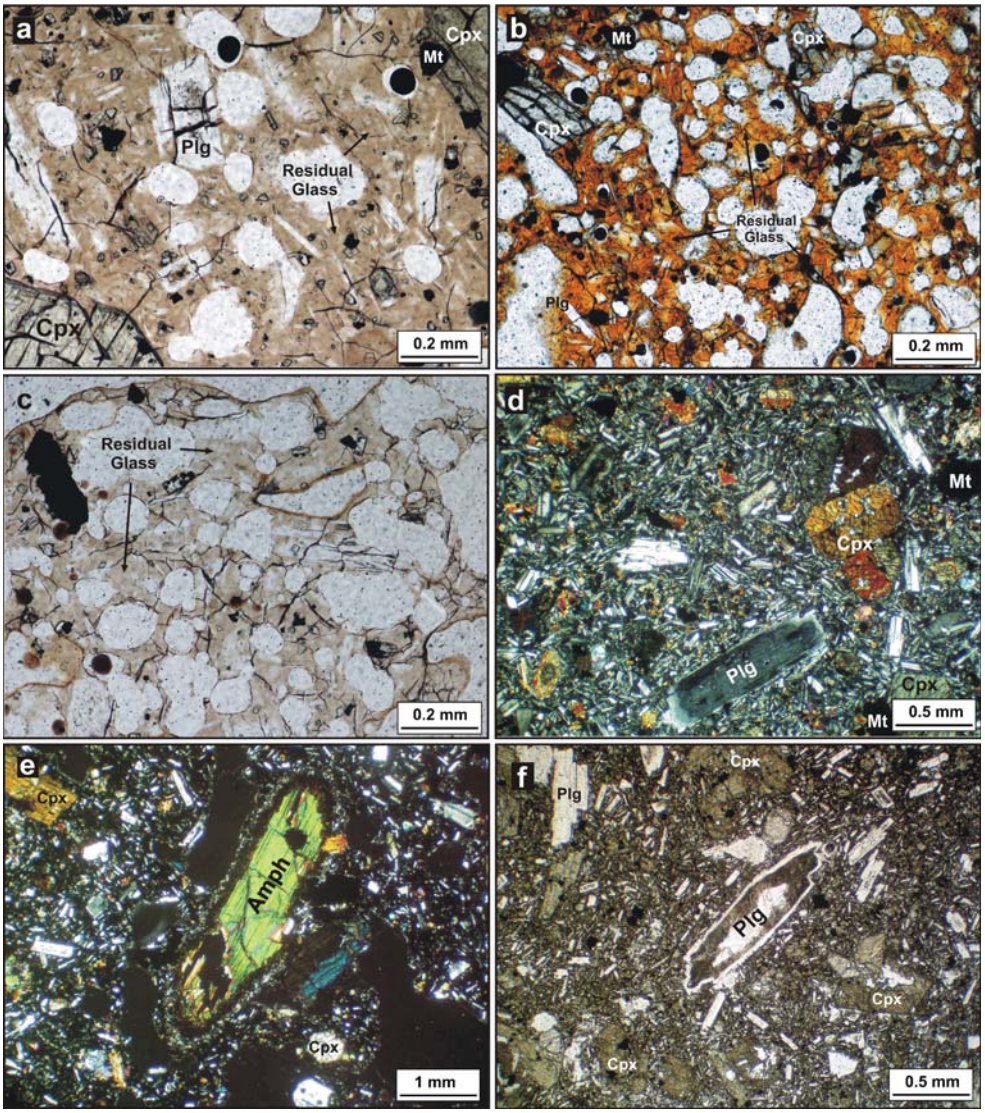

Fig. 3 **a** CAL 1 tephra: plagioclase (*Plg*), augite (*Cpx*), Ti-magnetite (*Mt*) phenocrysts in abundant light gray sideromelane (*residual glass*) with scarce vesicles (<50 vol.%); **b** LAG 3 tephra: augite, Ti-magnetite, and plagioclase phenocrysts in abundant vesiculated orange tachylyte; **c** LAG 7 tephra: plagioclase, augite, olivine, and Ti-magnetite microlites in clear and highly vesiculated (>50 vol. %) sideromelane (a, b, c: parallel Nicols); **d** Lava sampled at the CAL scoria cone characterized by mesophyric seriate texture with plagioclase, augite, and Ti-magnetite phenocrysts in microcrystalline groundmass (crossed Nicols); **e** Isolated euhedral amphibole crystal in CAL lava showing a characteristically semi-opaque rim and sparse augite phenocrysts. Plagioclase, augite and scarce olivine, and Ti-magnetite are also present in the intersertal groundmass (crossed Nicols); **f** Lava sampled at the base of the Laghetto cone (LAG 7) characterized by mesophyric seriate texture with plagioclase, augite, olivine, and Ti-magnetite phenocrysts in microcrystalline groundmass (parallel Nicols) showing quite similar features compared to CAL products. Sieve-textured plagioclase is more abundant in LAG products than in CAL ones

Concentrations of TiO_2, FeO, and, to a minor extent, P_2O_5 show a moderate increase from the CAL 1 to LAG 3 and LAG 7 (Fig. 4a). The most important difference of residual glass compositions relates to K_2O and Cl contents (Fig. 4b; Table 1). They show a substantial and progressive increase from the CAL 1 to LAG 7 tephra layers, strictly correlated with the time-evolution of the eruption. The ranges of MgO and CaO concentrations are instead relatively similar in all of the analyzed levels, whereas only Na_2O concentrations are higher in CAL 1. However, a significant variability was observed for what concerns in particular MgO and K_2O contents of LAG 7 samples, suggesting a quite heterogeneous character of the melt even at millimeter-scale.

Petrography and petrology of lavas

Lavas of C–L system are moderately porphyritic with a seriate texture and Porphyricity Index (P.I.) generally ranging between 10 and 20 (rarely up to 30). CAL and LAG lavas are rather similar. Among their phenocrysts, augite is the most abundant (ca. 7–8 vol.%), followed by plagioclase (ca. 6–7 vol.%), olivine (ca. 3 vol.%), Ti-magnetite (ca. 2 vol.%), and amphibole (ca. 2–3 vol.%; Fig. 3d, e). Augite and plagioclase are generally euhedral with sizes ranging from 100–150 μm up to ~1 cm. Olivine and Ti-magnetite are from subhedral to euhedral, reaching the maximum size of about 100–200 μm. Plagioclase phenocrysts with sieve-textured cores and with An-enriched rims are more abundant in LAG lavas than in CAL ones (Fig. 3f). Amphibole is often megacrystic (up 8 cm long), due to a fast growth in a volatile-rich environment (Clocchiatti and Tanguy 2001; Clocchiatti et al. 2004; Corsaro et al. 2007; Viccaro et al. submitted), and with poikilitic texture, mainly enclosing plagioclase and augite. Most of the amphibole crystals show a characteristic semi-opaque envelope (~0.2 mm thick at maximum) probably due to dehydration related to eruptive decompression

Table 1 Major element analyses (wt%) of glass in tephra of the 2001 eruption at the C–L system

	SiO_2	TiO_2	Al_2O_3	FeO	MgO	MnO	CaO	Na_2O	K_2O	P_2O_5	Total	Cl
CAL 1												
Sample 1	50.99	1.96	16.46	10.72	3.31	0.21	7.53	4.19	3.34	1.05	99.77	0.21
Sample 2	50.95	1.91	16.64	10.71	3.27	0.14	7.46	4.32	3.52	0.82	99.74	0.22
Sample 3	50.87	2.13	16.70	10.46	3.24	0.20	7.44	4.22	3.56	0.95	99.79	0.17
Sample 4	51.00	2.02	16.64	10.58	3.26	0.16	7.50	4.25	3.40	0.97	99.78	0.19
Sample 5	50.90	1.99	16.38	10.83	3.20	0.26	7.45	4.36	3.50	0.91	99.79	0.18
Sample 6	51.02	2.01	16.64	10.87	3.22	0.15	7.45	3.99	3.49	0.90	99.74	0.21
Sample 7	51.12	1.97	16.68	10.51	3.22	0.18	7.35	4.30	3.52	0.93	99.77	0.20
Sample 8	51.17	2.00	16.63	10.46	3.07	0.20	7.44	4.32	3.66	0.91	99.85	0.14
Sample 9	50.80	1.98	16.76	10.50	3.29	0.16	7.50	4.36	3.49	0.91	99.76	0.21
Sample 10	51.20	2.04	16.81	10.81	3.16	–	7.40	3.89	3.65	0.87	99.83	0.14
Averaged	51.00	2.00	16.63	10.64	3.22	0.19	7.45	4.22	3.51	0.92	99.80	0.19
1σ	±0.13	±0.06	±0.13	±0.16	±0.07	±0.04	±0.05	±0.16	±0.10	±0.06		±0.03
LAG 3												
Sample 1	51.80	2.17	17.03	10.90	3.36	0.15	6.34	3.23	3.92	0.93	99.84	0.17
Sample 2	51.48	2.16	17.04	11.05	3.22	0.21	6.01	3.56	4.01	0.98	99.73	0.26
Sample 3	52.18	1.91	16.92	11.22	3.23	0.16	6.46	2.90	3.95	0.85	99.80	0.19
Sample 4	51.37	1.85	16.58	11.34	3.39	–	5.82	4.11	4.65	0.91	100.01	0.21
Sample 5	50.51	1.94	18.16	10.71	2.99	–	6.19	4.19	4.19	1.13	100.00	0.18
Sample 6	51.96	2.08	16.84	10.73	3.33	–	6.93	2.67	4.13	1.11	99.78	0.20
Sample 7	51.68	1.99	16.86	11.38	3.26	0.24	6.60	2.74	4.10	0.98	99.82	0.20
Sample 8	51.66	2.18	16.96	11.22	3.36	0.28	6.05	3.26	3.93	0.84	99.74	0.24
Sample 9	51.47	1.99	16.82	10.72	3.17	0.16	7.29	3.41	3.85	0.88	99.76	0.24
Sample 10	51.72	2.04	16.91	11.00	3.20	0.19	6.25	3.35	4.06	1.03	99.75	0.24
Sample 11	51.60	2.04	16.77	10.71	3.19	0.26	7.80	2.83	3.62	0.98	99.80	0.20
Sample 12	52.22	2.09	17.01	10.92	3.09	0.22	7.11	2.52	3.64	0.98	99.80	0.20
Sample 13	51.69	2.18	17.08	11.31	3.27	0.30	7.16	2.35	3.62	0.91	99.86	0.14
Sample 14	52.04	2.03	17.15	10.86	3.28	0.19	6.16	3.12	4.07	0.90	99.81	0.18
Sample 15	51.93	2.16	16.99	11.07	3.27	–	6.59	3.05	3.90	0.86	99.81	0.19
Averaged	51.69	2.05	17.01	11.01	3.24	0.22	6.58	3.15	3.98	0.95	99.88	0.20
1σ	±0.41	±0.10	±0.35	±0.24	±0.11	±0.05	±0.56	±0.53	±0.26	±0.09		±0.03
LAG 7												
Sample 1	51.46	2.14	16.52	10.98	3.17	0.20	6.47	3.03	4.85	0.91	99.74	0.28
Sample 2	51.42	2.11	16.63	10.85	3.09	–	5.53	3.84	5.38	0.93	99.79	0.27
Sample 3	51.74	2.11	16.65	11.53	3.57	0.18	4.54	3.15	5.23	1.02	99.73	0.30
Sample 4	51.14	2.07	16.99	11.30	2.67	–	5.06	4.27	5.39	0.89	99.78	0.26
Sample 5	50.15	2.14	16.45	10.90	2.76	0.16	6.91	4.31	5.06	0.91	99.75	0.29
Sample 6	51.65	2.26	16.77	11.27	3.36	0.26	5.46	2.85	4.83	0.97	99.69	0.33
Sample 7	50.81	2.19	16.52	11.43	2.99	0.14	6.30	3.44	4.92	1.04	99.78	0.27
Sample 8	50.93	2.07	16.54	11.17	2.48	0.24	5.95	4.39	4.97	0.97	99.73	0.30
Sample 9	51.95	2.18	16.67	10.79	3.12	0.21	6.04	2.97	4.79	1.03	99.74	0.29
Sample 10	51.19	2.12	16.58	10.91	3.40	0.28	4.48	4.23	5.56	1.01	99.77	0.29
Averaged	51.24	2.14	16.63	11.11	3.06	0.21	5.68	3.65	5.10	0.97	99.79	0.29
1σ	±0.53	±0.06	±0.15	±0.26	±0.34	±0.05	±0.81	±0.62	±0.27	±0.05		±0.02

Samples represent different grains from each tephra layer.

(Fig. 3e). These rims are generally composed by a mixture of fassaite, rhönite, and anorthite with an interstitial K-rich residual glass (cf. Clocchiatti and Tanguy 2001; Clocchiatti et al. 2004). The mesostasis is hyaline to microcrystalline, being in general intersertal to hyalopilitic with variable volume percent of glass. The microlites are mainly plagioclase, scarce augite, and olivine, with Ti-magnetite and apatite as minor phases. Readers can refer to Clocchiatti et al. (2004) and Viccaro et al. (2006) for more detailed treatment of the chemistry of mineral phases for both major and trace elements.

Major element data have been analyzed by wavelength dispersive x-ray fluorescence (WD-XRF) at the Dipartimento di Scienze della Terra of Cosenza (University of Calabria, Italy). FeO content was analysed by $KMnO_4$ titration. Results obtained (Table 2) are comparable with

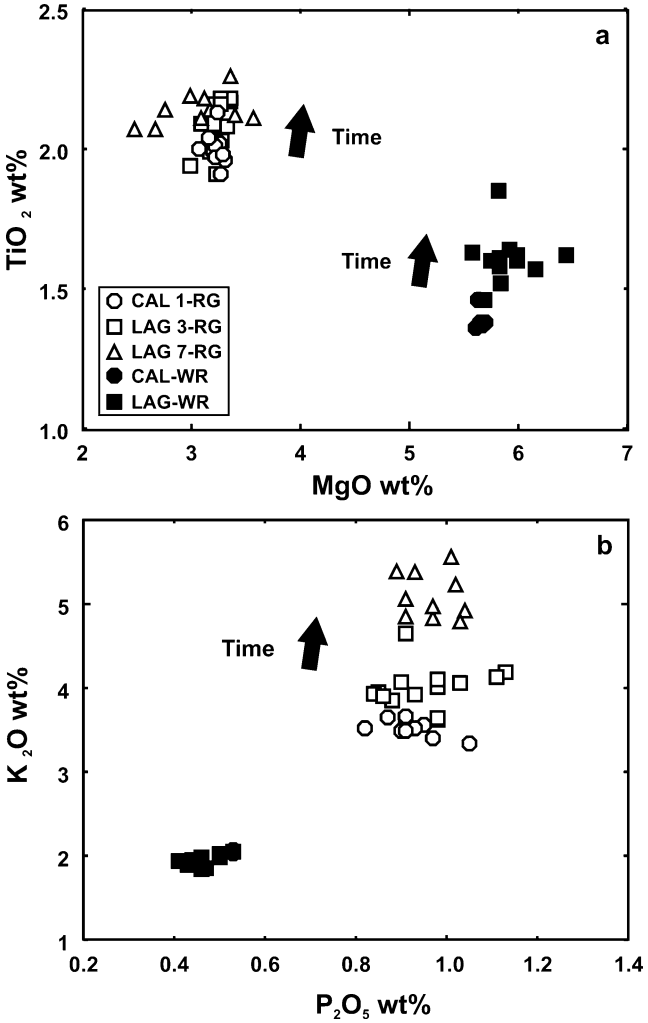

Fig. 4 **a** MgO vs TiO_2 and **b** P_2O_5 vs K_2O diagrams (wt%) for CAL and LAG products (*RG* residual glass in tephra; *WR* lava whole rock). CAL-WRs represent the first emitted lavas (July 18) at the CAL vent. LAG-WRs represent the intermediate and final emitted lavas at the LAG vent. CAL-RG are glass compositions representing the first eruptive phase of the C–L system at the CAL vent. LAG 3-RG are glass compositions representing the intermediate phase of eruptive activity of the C–L system at the LAG vent. LAG 7-RG are glass compositions representing the last eruptive phase of the C–L system at LAG vent

previously published data of the C–L system lavas (Clocchiatti et al. 2004; Métrich et al. 2004) but systematically differ from those of Viccaro et al. (2006) for their slightly lower SiO_2 and Al_2O_3 contents, with only minor differences for the other oxides.

All of the C–L lavas are trachybasalts (Le Maitre 2002) similar to the vast majority of rocks erupted recently on Mount Etna with a rather limited variability in major element abundances (Barbieri et al. 1993; Corsaro and Cristofolini 1996; Cristofolini and Romano 1982; Cristofolini et al. 1981; Tanguy et al. 1997; Figs. 4; Table 2). A careful examination of major element variation for C–L lavas reveals regular changes related to space and time. In detail, CAL lavas are slightly more silicic and very homogeneous in their compositions compared to the LAG ones, which are more basic and heterogeneous (Fig. 4). This variability is similar to that reported by Viccaro et al. (2006).

Discussion

Differentiation process

The compositional variability among the lavas erupted by the C–L fracture system during the 2001 eruption (Fig. 5) has been interpreted by Viccaro et al. (2006) as due to the mixing of the amphibole-bearing ABT magma with a more basic and deeper end-member (DBM). Products derived by the mixing process (LAG 3 and LAG 7 in this work) were exclusively erupted at the Laghetto vent towards the intermediate and later phases of the eruption.

The data on major element distribution in the lava whole rocks (WRs) and in the tephra residual glasses (RGs) show ample compositional differences. All of the lava WRs are trachybasalts, whereas most of the tephra RGs are more evolved, with basaltic-trachyandesites compositions in CAL 1, LAG 3, and phono-tephritic in LAG 7. RGs from the three levels, referred, respectively, to the initial, intermediate, and final phases of the eruption, are clearly distinct from each other (Fig. 4). In the CAL products, differences between WR and RG compositions are relatively small (ΔMgO ~2.5 wt%; ΔK_2O ~1.6 wt%). Variability is slightly higher between LAG 3-RGs and the related LAG-WRs thus displaying the largest differences between final phase LAG-WRs and LAG 7-RGs. Furthermore, these glasses display values distributed over a rather wide range (K_2O 4.8–5.7 wt%; TiO_2 1.8–2.3 wt%, and MgO ~2.5–3.4 wt%; Figs. 4 and 5).

The role of crystal fractionation in producing the observed compositional gap was tested by means of major element mass balance calculations (Stormer and Nicholls 1978) for both CAL and LAG products. Data on CAL 1-WR and LAG 17-WR (the most basic lavas with P.I. ~10) were chosen as starting compositions and averaged compositions of residual glasses of the CAL 1 and LAG 7 tephra layers as final composition. Compositions at the rim of plagioclase, augite, olivine, and Ti-magnetite phenocrysts in CAL 1-WR and LAG 17-WR have been chosen for mass balance calculations (data source Viccaro et al. 2006), as they should represent conditions close to thermodynamic equilibrium with the residual melt. Data used in mass balance calculations are shown in Table 3.

Results show that CAL-RGs may be derived from the CAL-WRs subtracting ~37% by weight solid phases (phenocrysts and microlites, namely, plagioclase, augite, olivine, and Ti-magnetite) with a sum of squared residuals

Table 2 Whole rock analyses of C–L lavas relative to the 2001 eruption and of the DBM

Sample	1 CAL	2 CAL	3 CAL	4 CAL	5 CAL	6 LAG	7 LAG	8 LAG	9 LAG	10 LAG	11 LAG	12 LAG	13 LAG	14 LAG	15 LAG	16 LAG	17 LAG	DBM
Date	18/7	18/7	18/7	18/7	18/7	26/7	26/7	26/7	27/7	27/7	27/7	28/7	28/7	29/7	29/7	30/7	30/7	
	CAL 1	CAL 1	CAL 1	CAL 1	CAL 1	LAG 3	LAG 3	LAG 3	LAG 3	LAG 3	LAG 3	LAG 3	LAG 3	LAG 7	LAG 7	LAG 7	LAG 7	
SiO_2	48.54	48.64	48.56	48.71	48.81	47.58	47.66	47.87	47.74	47.80	47.63	47.66	47.69	47.75	47.79	47.39	47.30	47.06
TiO_2	1.47	1.39	1.38	1.37	1.36	1.61	1.58	1.64	1.53	1.47	1.65	1.62	1.61	1.59	1.61	1.63	1.63	1.80
Al_2O_3	18.02	18.01	18.26	18.40	18.33	17.91	17.53	17.48	17.93	18.22	17.34	17.49	17.49	17.61	17.36	17.40	17.23	17.41
FeO_{tot}	9.21	8.87	8.74	8.68	8.67	10.10	10.18	10.30	9.47	9.23	10.38	9.97	10.16	9.93	10.14	10.39	10.65	10.59
MnO	0.17	0.17	0.16	0.16	0.16	0.18	0.18	0.19	0.17	0.17	0.19	0.18	0.19	0.18	0.19	0.19	0.19	0.18
MgO	5.66	5.72	5.67	5.69	5.63	5.78	6.20	5.60	5.87	5.71	5.95	5.85	5.78	5.86	6.02	6.02	6.47	5.87
CaO	10.36	10.49	10.29	10.10	10.20	11.07	11.01	11.21	10.83	10.70	11.26	10.91	11.13	10.99	11.04	11.36	10.97	11.19
Na_2O	4.00	4.14	4.32	4.27	4.22	3.42	3.35	3.31	3.98	4.11	3.24	3.79	3.52	3.65	3.44	3.29	3.24	3.42
K_2O	2.04	2.05	2.08	2.08	2.08	1.92	1.85	1.96	1.99	2.06	1.95	2.03	1.96	1.99	1.96	1.86	1.90	2.05
P_2O_5	0.53	0.53	0.53	0.53	0.53	0.44	0.46	0.44	0.50	0.53	0.41	0.50	0.46	0.46	0.44	0.47	0.43	0.43
Fe_2O_3	5.79	3.58	3.25	3.33	2.74	4.90	5.83	4.23	4.54	3.73	4.90	4.26	5.81	4.50	5.40	5.03	5.15	5.28
FeO	3.95	5.62	5.79	5.65	6.18	5.64	4.87	6.45	5.34	5.84	5.92	6.09	4.87	5.83	5.23	5.81	5.96	5.84

Lavas 1–5 CAL are equivalent to products of the CAL 1 tephra layer, 6–13 LAG lavas to the LAG 3 and 14–17 LAG lavas to the LAG 7.

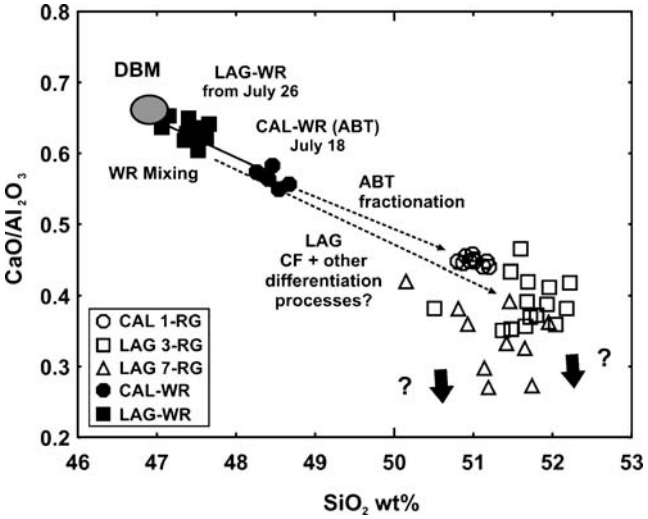

Fig. 5 SiO_2 vs CaO/Al_2O_3 diagram (wt%) displaying the complex evolution of lavas and tephra of the 2001 eruption. LAG-WRs appear as derived by mixing of the ABT magma (represented by CAL-WRs) with a deep basic end-member (*DBM*; from Viccaro et al. 2006). The DBM composition inferred by the previous authors matches fairly well those of most primitive Etnean products (cf. Armienti et al. 1989) and those of products recently erupted during the 2004–2005 event (Viccaro 2006; cf. Corsaro and Miraglia 2005). As regards differences between CAL-WRs and CAL-RGs, they can be accounted for by simple crystal fractionation (Table 3), whereas differences between LAG-WRs and LAG-RGs are larger and cannot be regarded as due to crystal fractionation (see text for discussion; Table 3)

(SSR) close to unit (Table 3). The outcome is consistent with differentiation by crystallization of the magma erupted from the CAL vent. Similar mass balance calculations for LAG-WRs and related LAG-RGs did not produce significant results (Table 3), thus implying that the simple subtraction of phenocrysts is not in accord with the observed RG compositions (Fig. 5). Other differentiation processes must therefore be considered, which acted only on the magma erupted at the Laghetto vent during the final phase of the event.

Considering that mixed ABT-DBM products were erupted at the Laghetto cone (Viccaro et al. 2006), a model was also tested, which assumes chemical variations as solely due to mixing of different proportions of these end-members. A thermodynamic approach with the MELTS code (release v5.0; Ghiorso and Sack 1995; Asimow and Ghiorso 1998) was then performed, using geophysical and petrological data to constrain the chemical and physical parameters of both magmas and consequently, the depth at which mixing could have occurred (Bonaccorso et al. 2004; Patanè et al. 2002; Billi et al. 2003; Lanzafame et al. 2003; Métrich et al. 2004; Monaco et al. 2005; Viccaro et al. 2006). The composition of DBM end-member is only hypothetical, as this magma was never erupted during the 2001 event. The composition chosen for the DBM that compares well with Etnean primitive magmas (Armienti et al. 1989), fitting the characters required to be an end-

Table 3 Results of mass balance calculations for major elements

	SiO_2	TiO_2	Al_2O_3	FeO	MnO	MgO	CaO	Na_2O	K_2O	P_2O_5	Total	Solid removed %	Liquid %	SSR
CAL1 mass balances														
Initial Liq														
1CAL-WR	48.54	1.47	18.02	9.21	0.17	5.66	10.36	4.00	2.04	0.53	100.00			1.01
Final Liq														
CAL1-RG	51.00	2.00	16.63	10.64	0.17	3.22	7.45	4.22	3.51	0.92	99.78		63.3	
Plg														
An_{87}	46.39	0.14	32.90	0.63			17.86	1.30	0.21		99.43	−22.0		
Cpx														
Wo_{46}-En_{39}-Fs_{15}	48.83	1.29	4.75	9.57	0.25	13.38	22.04	0.05	0.21		100.37	−7.3		
Ol														
Fo_{71}	37.24	0.11		25.87	0.53	35.45	0.33		0.10		99.63	−7.3		
Ti-mt		14.28	5.22	76.10	0.58	2.89	0.15		0.12		99.34	−0.1		
Total												−36.7		
LAG7 mass balances														
Initial Liq														
17LAG-WR	47.30	1.63	17.23	10.65	0.19	6.47	10.96	3.24	1.90	0.43	100.00			1.66
Final Liq														
LAG7-RG	51.24	2.14	16.63	11.11	0.17	3.06	5.68	3.65	5.10	0.97	99.75		39.1	
Plg														
An_{77}	51.29	0.09	30.32	0.73			14.82	2.11	0.49		99.85	−32.4		
Cpx														
Wo_{47}-En_{40}-Fs_{13}	49.25	1.18	4.76	8.18	0.13	13.86	22.84		0.20		100.40	−17.1		
Ol														
Fo_{79}	38.29	0.10		19.21	0.30	41.19	0.35		0.14		99.58	−6.8		
Ti-mt		10.00	5.70	76.69	0.41	4.30	0.10				100.20	−4.6		
Total												−60.9		

Compositions of the mineral phases from Viccaro et al. (2006).
Plg Plagioclase; *Cpx* augite; *Ol* olivine; *Ti-mt* Ti-magnetite.

member in the mixing, is provided by the lavas of 2004–2005 eruption (Table 2), which represent the most basic terms of the eruptive period 2001–2005 (Viccaro 2006; cf. Corsaro and Miraglia 2005). DBM is to be considered almost aphyric during the mixing, that is, at near-liquidus conditions, because no phenocryst cores consistent with its composition are found in the LAG lavas (Viccaro 2006). DBM conditions were consequently set at T=1,100°C and P=200 MPa; the fO_2 of the magma is assumed to be buffered by quartz-fayalite-magnetite (QFM). Under these conditions, the computed stable assemblage is constituted by ~97 vol.% of liquid and ~3 vol.% of olivine and augite. The stable assemblage and thermodynamic properties of the ABT magma were calculated at T=990°C, P=200 MPa, and fO_2 at QFM buffer. These conditions lead to a stable assemblage constituted of ~58 vol.% of liquid, ~25 vol.% of augite, ~10 vol.% of plagioclase (An_{71}), ~4 vol.% of magnetite, ~3 vol.% olivine (Fo_{72}), and trace of apatite. This assemblage matches fairly well the petrography described in this work and by previous authors (Clocchiatti et al. 2004; Métrich et al. 2004; Viccaro et al. 2006). Due to the poor reliability of MELTS in dealing with hydrous phases, amphibole was not included in the simulation.

The mixing process was then simulated by modeling an isenthalpic assimilation between the two magmas, running the computing cycles until the system attained new thermodynamic equilibrium conditions. LAG-RG compositions and theoretical liquid compositions obtained from MELTS of the intermediate terms of the mixing were then transformed into molar proportions (Table 4).

Binary molar diagrams show that only Mg and to a minor extent Ca concentrations fall close to the calculated isenthalpic-mixing curve between the ABT and DBM end-members, therefore the variation for these elements can be ascribed to mixing (Fig. 6). Elements such as Al and Na do not fit the theoretical isenthalpic-mixing curve, which means that, besides mixing, other processes took part into the chemical evolution that modified the composition of LAG-RGs. The possible contribution of mineral fractionation in modifying the contents of Al, Mg, Ca, and Na was determined by using "MINUIT-Function minimization and error analysis" (version 2.77 © copyright CERN Geneva 1994–1998; see Appendix 1 for details of calculations). The results indicate that the subtraction of ~0.29 g of solid for each gram of melt (namely, plagioclase and very scarce olivine) from the theoretical compositions of the mixed melt (~30% DBM) can produce LAG 7-RGs (Fig. 6). Results match reasonably well the petrographic features. Patches of LAG glasses are in fact characterized by microlites mostly of plagioclase and scarcer olivine (Fig. 3c), nucleated under pre- to syn-eruptive conditions, which could likely have affected the composition of the surrounding glass. Other elements such as Ti, Fe, P, and K neither match the theoretical isenthalpic-mixing curve (Fig. 6) nor is the variability consistent with a late crystallization of any mineral phase (see Appendix 1). This suggests that these processes are not sufficient to account for the observed changes. In addition, the distribution of MgO in LAG 7-RGs is variable. This can only be explained by admitting certain heterogeneity of the melt, even at millimetric scale, consistent with an incomplete mixing of the two end-members. However, immiscibility must not have been significant, as the two magmas were compositionally close. The preservation of the heterogeneous glass geochemistry is most likely to be related to the high rate of mixing and simultaneous eruption. More importantly, the averaged K_2O content ranges from ~3.5 wt% in the CAL 1-RGs up to 5.1 wt% in LAG 7-RGs. This K enrichment displays a positive correlation with the timing of the eruptive event and reaches a peak just in the uppermost tephra levels of the Laghetto cone (Fig. 7).

The enrichment of the glass in K and other elements is too high and not consistent with any common interpretation of differentiation processes such as fractionation and magma mixing. Another differentiation process of the magmas residing within the plumbing system of the Etnean volcano is therefore required to interpret the observed composition of the LAG-RGs.

The role of volatiles migration

Volatiles easily migrate in a volcanic environment with a transfer efficiency chiefly depending on partial pressure gradients and on the extent of microfracture systems. At Mount Etna, the efficient transfer of great amounts of magmatic volatiles (i.e., averaged SO_2 flux 4,000 ton day^{-1}) is demonstrated by the steady-state degassing of the convectively moving magma column that fills the open conduit system and by the fumarole network distributed in the upper section of the volcanic edifice (Allard et al. 1991; Allard 1997; Métrich and Rutherford 1998). Volatile migration can involve the transfer of metallic elements which have a particular affinity with H_2O and halogens, due to the crucial role of halogens as complexing agents. Cl^- in particular is able of extracting from the melt, as complexes, significant amounts of metals and other elements (i.e., H, K, Ti, Fe) and other complexes found in fumarolic gases (Symonds et al. 1994 and reference therein; Kodosky and Keith 1993; Shinohara et al. 1989 and references therein).

The plumbing system before the 2001 eruption under the Laghetto can be reconstructed using petrological, geophysical, and geochemical data (Bonaccorso et al. 2002, 2004; Caracausi et al. 2003a, b; Métrich et al. 2004; Monaco et al. 2005; Viccaro et al. 2006). Below the Laghetto area in the

Table 4 Results (molar proportion) of isenthalpic mixing simulations between ABT and DBM

	SiO_2	TiO_2	Al_2O_3	FeO	MnO	MgO	CaO	Na_2O	K_2O	P_2O_5
ABT	0.602	0.005	0.146	0.046	0.002	0.034	0.066	0.071	0.026	0.004
LAG 5% Mixing	0.596	0.005	0.143	0.048	0.002	0.039	0.070	0.068	0.025	0.004
LAG 10%	0.591	0.006	0.140	0.050	0.002	0.043	0.074	0.066	0.025	0.004
LAG 15%	0.587	0.006	0.138	0.051	0.002	0.046	0.078	0.064	0.024	0.003
LAG 20%	0.583	0.007	0.137	0.052	0.002	0.049	0.080	0.063	0.024	0.003
LAG 25%	0.579	0.007	0.135	0.054	0.002	0.052	0.082	0.062	0.023	0.003
LAG 30%	0.575	0.008	0.133	0.056	0.002	0.055	0.086	0.060	0.023	0.003
LAG 35%	0.571	0.008	0.131	0.059	0.002	0.057	0.089	0.058	0.022	0.003
LAG 40%	0.567	0.009	0.130	0.061	0.002	0.060	0.091	0.057	0.021	0.003
LAG 45%	0.564	0.009	0.128	0.063	0.002	0.062	0.093	0.056	0.021	0.003
LAG 50%	0.561	0.009	0.127	0.065	0.002	0.063	0.095	0.055	0.020	0.003
DBM	0.518	0.014	0.118	0.090	0.002	0.082	0.122	0.038	0.014	0.002
LAG3										
Sample 1	0.572	0.018	0.111	0.101	0.001	0.055	0.075	0.035	0.028	0.004
Sample 2	0.571	0.018	0.111	0.102	0.002	0.053	0.071	0.038	0.028	0.005
Sample 3	0.576	0.016	0.110	0.104	0.001	0.053	0.076	0.031	0.028	0.004
Sample 4	0.567	0.015	0.108	0.105	–	0.056	0.069	0.044	0.033	0.004
Sample 5	0.562	0.016	0.119	0.100	–	0.050	0.074	0.045	0.030	0.005
Sample 6	0.574	0.017	0.110	0.099	–	0.055	0.082	0.029	0.029	0.005
Sample 7	0.571	0.017	0.110	0.105	0.002	0.054	0.078	0.029	0.029	0.005
Sample 8	0.571	0.018	0.111	0.104	0.003	0.055	0.072	0.035	0.028	0.004
Sample 9	0.568	0.017	0.109	0.099	0.001	0.052	0.086	0.036	0.027	0.004
Sample 10	0.573	0.017	0.110	0.102	0.002	0.053	0.074	0.036	0.029	0.005
Sample 11	0.568	0.017	0.109	0.099	0.002	0.052	0.092	0.030	0.025	0.005
Sample 12	0.577	0.017	0.111	0.101	0.002	0.051	0.084	0.027	0.026	0.005
Sample 13	0.570	0.018	0.111	0.104	0.003	0.054	0.085	0.025	0.025	0.004
Sample 14	0.576	0.017	0.112	0.100	0.002	0.054	0.073	0.033	0.029	0.004
Sample 15	0.573	0.018	0.111	0.102	–	0.054	0.078	0.033	0.027	0.004
LAG7										
Sample 1	0.570	0.018	0.108	0.102	0.002	0.052	0.077	0.033	0.034	0.004
Sample 2	0.572	0.018	0.109	0.101	–	0.051	0.066	0.041	0.038	0.004
Sample 3	0.575	0.018	0.109	0.107	0.002	0.059	0.054	0.034	0.037	0.005
Sample 4	0.571	0.017	0.112	0.106	–	0.044	0.061	0.046	0.038	0.004
Sample 5	0.557	0.018	0.108	0.101	0.001	0.046	0.082	0.046	0.036	0.004
Sample 6	0.574	0.019	0.110	0.105	0.002	0.056	0.065	0.031	0.034	0.005
Sample 7	0.565	0.018	0.108	0.106	0.001	0.050	0.075	0.037	0.035	0.005
Sample 8	0.568	0.017	0.109	0.104	0.002	0.041	0.071	0.047	0.035	0.005
Sample 9	0.576	0.018	0.109	0.100	0.002	0.052	0.072	0.032	0.034	0.005
Sample 10	0.570	0.018	0.109	0.102	0.003	0.056	0.053	0.046	0.039	0.005

Table shows the theoretical terms of the mixing (LAG) resulting from the incremental isenthalpic mixing between the ABT and DBM end members (from 5 to 50% of DBM involved) as well as the LAG 3 and LAG 7 glass compositions measured by SEM-EDS (molar proportion).

months preceding the eruption, there was a shallow magma body (ABT) residing at about 6 km b.s.l. and a deeper magma body (DBM) rising from ~10 km b.s.l. The DBM volatile content is assumed to be 3.4 wt% H_2O and 1,100 ppm CO_2, on the basis of data on primitive melt inclusions in olivine crystals erupted at the LAG vent (Métrich et al. 2004). Volatile saturation pressures indicate that ~70% of CO_2 had already exsolved from the magma at 400 MPa (Métrich et al. 2004). Similar conclusions, indicating degassing pressures in the range of 330–400 Mpa (corresponding to depths of ~8.5–10 km b.s.l.,) derive from CO_2 and noble gases measurements in the period preceding the 2001 eruption that indicate the input from depth of an undegassed magma (Caracausi et al. 2003b), which is likely related to the ascending DBM.

Calculations performed with VOLATILECALC (Newman and Lowenstern 2002) give a minimum pressure value of ~250 MPa for the coexistence with the DBM of a multicomponent (H_2O + CO_2) gas phase for a T of 1,100°C. This value of pressure indicates that volatiles were able to exsolve below the ABT magma chamber residing at ~200 MPa. Furthermore, the constraining pressure on DBM could drop below volatiles saturation level due to fracture opening, enhancing gas phase exsolution and migration. As the rate of

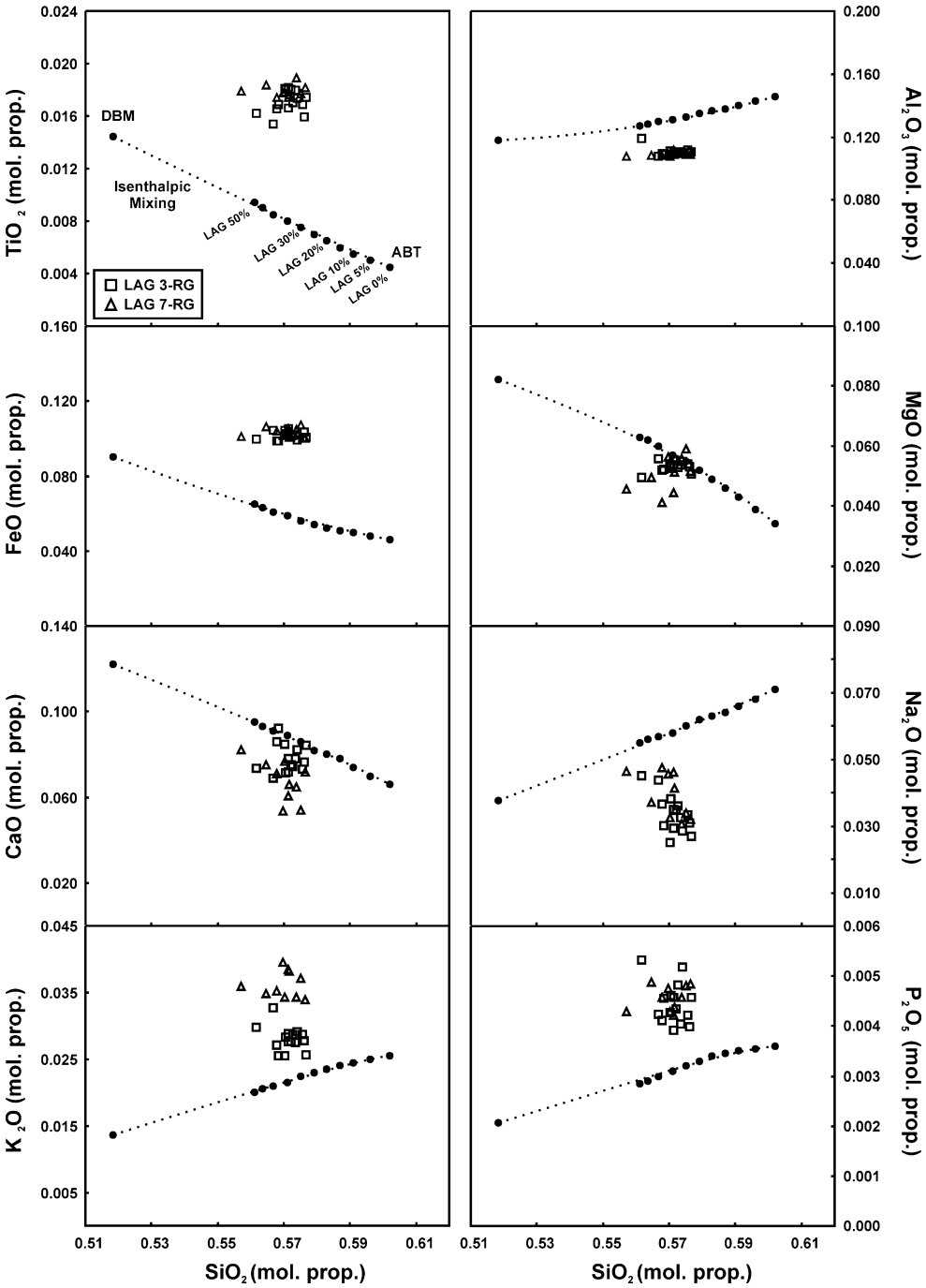

Fig. 6 SiO_2 vs oxide diagrams on the basis of molar proportions for terms involved in the mixing process (Table 4). In figure are shown the isenthalpic paths of magma mixing between ABT and DBM end-members calculated for each oxide with the assimilation function of the MELTS code. Simulations give the theoretical LAG compositions representing the mixed terms between the two considered end-members. Each step of the mixing path corresponds to an increment of 5% of the process, reflecting the addition of 10 g of mass of DBM to the ABT end-member. Analysed LAG 3 and LAG 7 glass compositions (in molar proportion) are also shown on the diagrams (see text for discussion)

volatiles migration primarily depends on the extension of the fractures network, when fractures are irregular and sufficiently narrow, the confining pressure of the magma is kept high enough to prevent a massive volatile exsolution, which could trigger magma ascent and consequent eruption. Migrating volatiles normally escape from the plumbing system reaching the surface as proven by the fumarolic fields. In the case of 2001, between the source of volatiles, represented by the DBM, and the surface there was the ABT magma chamber to potentially receive the migrating volatiles. However, the essential condition that can allow the redissolution of volatiles into the residing ABT magma is its undersaturation. This magma is a trachybasalt, similar to common Etnean magmas in terms of chemical composition and mineralogical assemblage. Volatile contents for these magmas are generally acknowledged to be H_2O ~2.5 wt% and CO_2 ~500 ppm at liquidus conditions (Armienti et al. 2002; Clocchiatti et al. 1992; Kamenetsky and Clocchiatti 1996). Calculations performed with VOLATILECALC indicate a minimum pressure of ~165 MPa for the coexistence of a multicomponent (H_2O + CO_2) gas phase with the ABT magma at T of 990°C. From this, it derives that at P

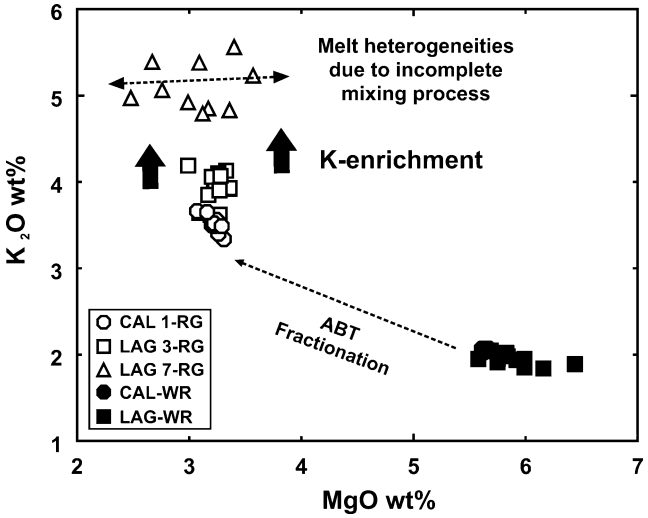

Fig. 7 MgO vs K_2O diagram (wt%) for CAL and LAG products. K shows a time-related enrichment in the intermediate and final levels of the LAG sequence. In addition, LAG 7-RGs display a marked dispersion which may be linked to small-scale heterogeneities related to an incomplete mixing. However, the strong K increase cannot be interpreted by simple subtraction of solid phases and magma mixing

of ~200 MPa (corresponding to ~6 km b.s.l.), ABT magma was probably undersaturated. The amphibole found in the ABT assemblage is not inconsistent with this conclusion, as amphibole can crystallize at P_{vol} below volatile saturation. Furthermore, it is suggested that the crystallization of amphibole was extremely localized and occurred only in the upper part of the magma chamber (Clocchiatti and Tanguy 2001; Clocchiatti et al. 2004; Corsaro et al. 2007; Viccaro et al. submitted).

High contents of mobile elements in tephra are concentrated in the uppermost tephra layers of the LAG sequence, erupted towards the end of the event. This is interpreted as an indication that the enrichment in Ti, Fe, P, and especially K occurred prevailingly in the lowest part of the erupted ABT magma body. Evidence that the element pattern of the tephra glasses could be related with the migration of volatiles is provided by the variation of Cl content. Abundance of Cl is positively correlated with all the enriched elements and particularly with K (Fig. 8).

The main chlorine compound in Etnean volcanic gases is HCl. However, sublimates found near the vents testify that elements such as alkalis, P, Ti, Fe, and other transition metals are easily transported and deposited by the volatile phase when it reaches the surface (Rittmann 1962; Le Guern and Bernard 1982). Moreover, Le Guern and Shinohara (1985) have found that, during the activity of 1983 at Mt. Etna, significant amount of alkali chlorides (e.g., KCl=1.2 wt%) were released by volcanic gases. In a magmatic system, the action of the halogens in complexing and carrying mobile elements strongly depends on T and P gradients (Rittmann 1962). As the plumbing system extends vertically for several kilometers, the physical conditions of the magma change so that gases will encounter different P and T conditions during their upward migration. As reactions of metal–halogens complexing are endothermic, elements transported in the gas phase redissolve into the magma at lower P and T, leading to an elemental transfer from the lower to higher portions of the magma storage zone.

Cl release into the gas phase depends on the melt composition and is greatly enhanced as the magma differentiates (Webster 2004; Webster et al. 1999; Webster and De Vivo 2002). Experimental results show that Cl solubility has negative pressure dependence, thus implying that if magma coexists with Cl-bearing gas, Cl dissolves into the melt during magma decompression (Signorelli and Carroll 2000; Carroll 2005 and references therein). The effects of negative pressure-dependence of Cl solubility are however not significant in basaltic melts saturated with hydrosaline solutions, for P ranging between 0.1 and 200 MPa (Webster et al. 1999; Bhalla et al. 2002).

Spilliaert et al. (2006) have recently pointed out that Cl begins to exsolve from the Etnean alkali basalts at pressure <100 MPa, with a degassing rate strongly dependent on the dynamics of magma ascent and extrusion (cf. also Métrich and Rutherford 1992; Gardner et al. 2006). In the Laghetto sequence, the increase in chlorine content from LAG 3 to LAG 7 layers is not accompanied by an evolution of residual glasses (Figs. 4, 5, and 7) and significant changes in the dynamics of extrusion, ruling out the possibility that such an enrichment could be an effect of fractionation or

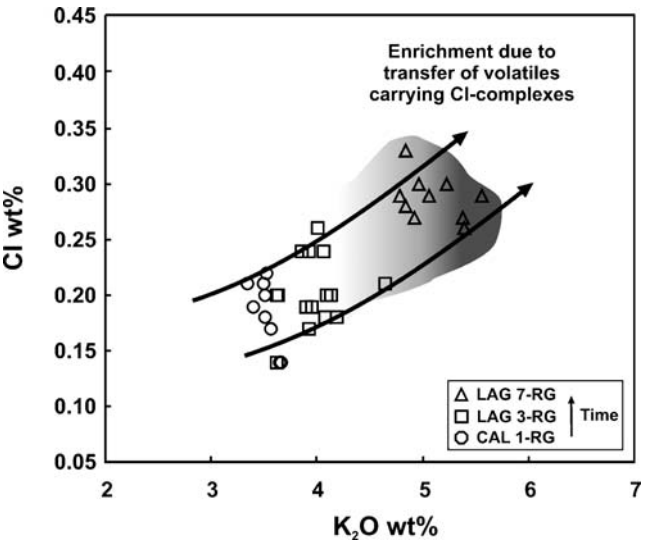

Fig. 8 K_2O vs Cl diagram (wt%) for CAL and LAG glass compositions of the sampled tephra sequence. The positive correlation between Cl and K, increasing both towards the upper layers of the Laghetto sequence, indicates the role played by volatiles in carrying Cl-complexes of Ti, Fe, P, and, in particular, of K

degassing during the magma ascent. Cl-enrichment must therefore be explained by a fluxing of a Cl-bearing gas phase into the ABT magma residing at 200 MPa. Given that chlorine as volatile component in Etnean alkali basalts begins to exsolve at pressure of <100 MPa (Spilliaert et al. 2006), its presence in the gas phase, exsolving from the DBM at ~250 MPa, reasonably occurs as Cl complexes of metallic elements such as K, Ti, Fe, and P. Recently, Beermann et al. (2006) investigated Cl solubility and fluid/melt partitioning in trachybasalts of the Etna 2001 eruption, setting experimental conditions at T=1150°C, P=200 MPa, and fO_2=QFM+1, similar to those inferred for the DBM. They demonstrated that under these conditions partitioning of chlorine strongly depends on the formation of complexes of K and other mobile elements extracted from the melt into the gas phase. Mobile elements transported with the migrating volatiles towards the upper portion of the plumbing system can therefore be dissolved again into the magma when they encounter lower P and T conditions of the volatile undersaturated ABT magma. In this scenario, the enrichment in Ti, Fe, P, and, in particular, K can be regarded as the result of a "volatile-induced differentiation" driven by chemical and physical gradients between magma bodies within the plumbing system (Fig. 9; see Appendix 2 for mass balance calculation).

Finally, it is noteworthy that the highest content of elements like K, Cl (and Ti, Fe, P) in tephra are found only in the uppermost beds of the Laghetto sequence erupted at the end of the event. This is a strong indication that their enrichment was rather limited, involving exclusively the lowest part of the erupted ABT magma body. This is consistent with the low volatile diffusivity in crystallizing magmas. Bachmann and Bergantz (2004) propose a rate of 10^{-9} m/s (~3 m per month) for well crystallized (~40%) silicic magmas. Even considering that the crystal fraction in the ABT reservoir was relatively little (~20 vol.%; "Petrography and chemistry of residual glass"), it seems likely that volatiles influx involved only the lowest portion of the magma chamber, having had not enough time to migrate upward probably due to the short time elapsed between the volatiles redissolution and the eruption onset. Specifically, after the seismic crisis of April 20 2001, the deformation pattern displayed a general deflation that is interpreted as originated by a relative loss of pressure of a magma body placed between 10 and 4 km b.s.l. (Bonaccorso et al. 2004 and references therein). The seismic crisis of April can therefore be interpreted as the beginning and triggering of the volatile migration from the DBM, suggesting that the volatiles influx entered the ABT magma for about 3 months.

Conclusive remarks

The stratigraphically controlled sampling of tephra layers related to the explosive activity of the 2001 eruption at Mount Etna has put in evidence the existence of complex

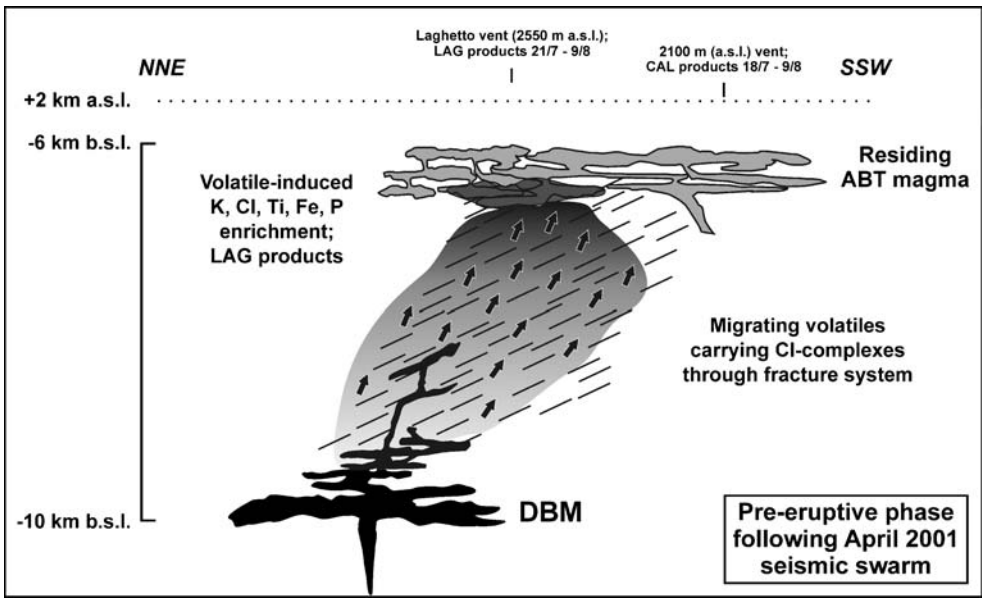

Fig. 9 Sketch model of the plumbing system in the months preceding the 2001 eruption at Mount Etna volcano. Volatiles (represented by the *shaded cloud* and *black arrows*), bearing Cl-complexes of K and other metallic elements, were able to exsolve and migrate upward from a deep seated magma (*DBM*) through fractures network developed probably following the earthquakes swarm of April 20 (Bonaccorso et al. 2004). The residing ABT magma gradually received these volatiles which induced enrichment in K, Cl, Ti, Fe, and P, thus originating the LAG products. The occurrence of this enrichment in the products erupted exclusively towards the end of the eruption at the Laghetto vent suggests that the "volatile-induced differentiation" process involved only the lower portion of the ABT magma chamber

differentiation processes acting within the feeding system of the volcano. Glass compositions of tephra display a time-related increase in Ti, Fe, P, and particularly in K and Cl contents, which are most noticeable at the top of the Laghetto sequence. Attempts to explain these enrichments in terms of traditionally employed models of differentiation processes, such as crystal fractionation and magma mixing, are not successful.

As an alternative, it is here suggested that volatiles composed of H_2O and CO_2 and Cl complexes of K, Ti, Fe, and P exsolved from a deep-seated magma body (DBM) and migrate upward through a fracture network developed at crustal level, very likely, originated by seismic events of the months preceding the onset of 2001 eruption. Volatile migration was blocked by a shallower residing magma (ABT), whose chemical and physical conditions permitted the dissolution of the gas phase thus producing the enrichment of the mobilized elements at the base of the magma chamber. Volatile influx in the period preceding the eruption increased the total volatile content in the basal level of the magma chamber. This had the consequence of greatly increasing the explosiveness of the short-lasting eruptive episode at the Laghetto vent towards the final phase of the eruption, which was one of the most violent in the last centuries.

Finally, this work advances the idea that volatile-induced differentiation, linked to primary petrological features of recent magmas, can contribute to the K enrichment observed in products erupted after 1971. Here, the mechanism has been highlighted on the scale of the individual eruption, but further data and improvements of the model probably might help to extend the role of volatiles to much broader issues at Mount Etna. A rigorous field-based approach systematically applied to products of past as well as future eruptions of Mount Etna and other alkali basaltic volcanoes may reveal anomalies and differences in compositions, otherwise overlooked, which can be attributed to processes controlled by volatile-induced differentiation.

Acknowledgments M.V. thanks G. Ottonello and M.S. Ghiorso for productive suggestions and discussions that significantly contributed to the quality of this work. Authors are grateful to M.A. Clynne, W.A. Bohrson, and an anonymous reviewer who provided perceptive and insightful reviews that improved the manuscript. R.A. Corsaro and L. Miraglia are greatly acknowledged for their technical assistance in SEM-EDS data acquisition at INGV-Sezione di Catania. Work supported by research grants from INGV-DPC (National Institute for Geophysics and Volcanology-Department of Civil Defence) and the University of Catania.

Appendix 1

Assuming that the isenthalpic mixing trend for each oxide (Fig. 6) is linear, we can define the slope of this line on each binary molar diagram as:

$$\mathrm{d}\,a/\mathrm{d}\,b \approx \Delta a/\Delta b$$

with a = any of the considered oxide and $b = SiO_2$.

Δa and Δb can be simply calculated as:

$$a_{\mathrm{LAG-RG1}} - a_{\mathrm{LAG-RG2}}$$

where $a_{\mathrm{LAG\text{-}RG1}}$ is the concentration of any oxide in the measured LAG residual glass representative of a given proportion of mixing, whereas $a_{\mathrm{LAG\text{-}RG2}}$ is the concentration of any oxide of the theoretical mixed term obtained from isenthalpic mixing simulations with MELTS representative of the same mixing proportion. Glasses of LAG layers are representative of the mixing, and the proportion chosen for the simulation are: 70% ABT and 30% DBM, according to Viccaro et al. (2006). Calculations were performed for all measured and calculated LAG residual glass compositions. However, in Table 5 are shown results

Table 5 Compositions (molar proportion) chosen for "MINUIT©" calculations

	SiO_2	TiO_2	Al_2O_3	FeO	MnO	MgO	CaO	Na_2O	K_2O	P_2O_5
LAG 30%	0.575	0.008	0.133	0.056	0.002	0.055	0.086	0.060	0.023	0.003
LAG7 Sample9	0.576	0.018	0.109	0.100	0.002	0.052	0.072	0.032	0.034	0.005
Δa		0.010	−0.024	0.044	0.000	−0.003	−0.014	−0.028	0.011	0.002
Δb	0.001									
Plg LAG7 Sample9	0.589	0.001	0.197	0.008	0.000	0.000	0.171	0.029	0.004	0.000
Cpx LAG7 Sample9	0.459	0.010	0.035	0.071	0.001	0.191	0.229	0.001	0.001	0.000
Ol LAG7 Sample9	0.329	0.001	0.000	0.168	0.004	0.494	0.004	0.000	0.001	0.000
Ti-mt LAG7 Sample9	0.000	0.095	0.041	0.782	0.004	0.076	0.001	0.000	0.000	0.000

Compositions refer to theoretical (MELTS) and natural glasses (Sample 9 from the LAG7 tephra layer) representing a mixing of 70% of ABT and 30% of DBM and the related mineral phases (from Viccaro et al. 2006). In Table are also shown the Δa and Δb values from which the contribution of each mineral phase for each oxide was calculated to set the matrix (See Appendix 1).

only from sample 9 LAG 7-RG with Δa and Δb values calculated for each oxide.

As four mineral phases (excluding amphibole) characterize products of the 2001 eruption, we can express the slope on each diagram (Fig. 6) with the general relation:

$$(\Delta a/\Delta b)_{M1}X_{M1} + (\Delta a/\Delta b)_{M2}X_{M2} + (\Delta a/\Delta b)_{M3}X_{M3} + (\Delta a/\Delta b)_{M4}X_{M4} = \Delta a/\Delta b \quad (1)$$

where M1 = plagioclase (Plg), M2 = augite (Cpx), M3 = olivine (Ol), M4 = Ti-magnetite (Ti-mt), and X_{M1}–X_{M4} represent their molar proportions. An example on the nine LAG 7-RG of mineral phase compositions in molar proportion used in the calculation are reported in Table 5 (source of data from Viccaro et al. 2006). Taking as an example TiO_2, from Eq. 1 we have:

$$(\Delta a_{TiO2}/\Delta b_{SiO2})X_{Plg} + (\Delta a_{TiO2}/\Delta b_{SiO2})X_{Cpx} + (\Delta a_{TiO2}/\Delta b_{SiO2})X_{Ol} + (\Delta a_{TiO2}/\Delta b_{SiO2})X_{Ti-mt} = \Delta a_{TiO2}/\Delta b_{SiO2}$$

Taking into consideration the contribution of each mineral phase for each oxide we obtain the following matrix:

$$TiO_2(0.010)X_{Plg} + (0.100)X_{Cpx} + (0.010)X_{Ol} + (0.950)X_{Ti-mt} = 10$$
$$Al_2O_3(-4.728)X_{Plg} + (-0.840)X_{Cpx} + (0)X_{Ol} + (-0.984)X_{Ti-mt} = -24$$
$$FeO(0.352)X_{Plg} + (3.124)X_{Cpx} + (7.392)X_{Ol} + (34.408)X_{Ti-mt} = 44$$
$$MgO(0)X_{Plg} + (-0.573)X_{Cpx} + (-1.482)X_{Ol} + (-0.228)X_{Ti-mt} = -3$$
$$CaO(-2.394)X_{Plg} + (-3.206)X_{Cpx} + (-0.056)X_{Ol} + (-0.014)X_{Ti-mt} = -14$$
$$Na_2O(-0.812)X_{Plg} + (-0.028)X_{Cpx} + (0)X_{Ol} + (0)X_{Ti-mt} = -28$$
$$K_2O(0.044)X_{Plg} + (0.011)X_{Cpx} + (0.011)X_{Ol} + (0)X_{Ti-mt} = 11$$
$$P_2O_5(0)X_{Plg} + (0)X_{Cpx} + (0)X_{Ol} + (0)X_{Ti-mt} = 2$$

Several minimization cycles performed with "MINUIT-Function minimization and error analysis (version 2.77 ©copyright CERN Geneva 1994–1998)" solve this matrix for the composition LAG 7-Sample 9 giving a total value of precipitated solid = 0.28 g for each gram of melt (plagioclase 92 wt%; olivine 8 wt%). Calculated masses of precipitated solid for LAG residual glasses range between 0.24 and 0.34 g. Microlites of plagioclase and olivine in the groundmass are in equilibrium with the compositions measured at phenocrysts rim. On the whole, plagioclase constitutes ~92% of solid and entirely balances Al, Ca, and Na concentrations, whereas the scarce olivine balances the slight differences observed for Mg (Fig. 6). Repeated cycles of function minimization do not balance the concentrations for other oxides, thus implying that a late fractionation of any of the considered mineral phases cannot be responsible to produce such variability.

Appendix 2

An attempt to quantify the volatiles needed to cause the observed variability can be done considering the ΔCl in moles (0.003) between averaged values of chlorine in the non "volatile differentiated" ABT (0.19 wt% in CAL 1) and the "volatile differentiated" LAG (0.29 wt% in LAG 7) on the basis of concentrations reported in Table 1. The amount of "volatile differentiated" magma in the ABT chamber can be conservatively assumed as the total volume of the material erupted in the very final phase of the event after the July 30 at the Laghetto vent. The volume of the last lava flow corresponds to about 240×10^3 m^3 (Ferlito and Siewert 2006). The DRE volume of tephra emitted in the last eruptive phase can be conservatively estimated assuming the thickness of the LAG 7 layer (10 m) and the dimension of the Laghetto scoria cone (Calvari and Pinkerton 2004) as no less than 260×10^3 m^3. The total volume of the "volatile differentiated" magma (500×10^3 m^3) corresponds to 6.1×10^{13} moles, on the basis of averaged oxide weight percent concentrations and the weighted proportion of mineral phases in LAG magma (Tables 2 and 3). For this amount of magma, the ΔCl_{tot} (the Cl needed to attain a concentration of 0.29 wt% starting from Cl 0.19 wt%) is equal to 1.8×10^{11} moles. The gas present in the system is here approximated to a multicomponent phase constituted by H_2O + CO_2 + Cl. The molar proportion of H_2O (~64 mol%) and CO_2 (~36 mol%) are derived using VOLATILECALC on the basis of volatiles concentration in melt inclusions (see "The role of volatiles migration" and Métrich et al. 2004) at P of 200 MPa and T 1,100°C. The Cl proportion in the gas phase is calculated considering the fluid/melt partitioning of Cl. The distribution of Cl between the fluid and the melt is generally expressed in the form of Nernst-type partition coefficients ($^{fluid/melt}D_{Cl}$) as:

$$^{fluid/melt}D_{Cl} = {}^{fluid}C_{Cl}/{}^{melt}C_{Cl}$$

Many authors have experimentally derived $^{fluid/melt}D_{Cl}$ for mafic melts at pressure of our interest (200 MPa) providing a wide range of values (0.9–18; Webster et al. 1999; Signorelli and Carroll 2000; Métrich et al. 2001; Wehrmann 2005; Alletti et al. 2006; Bhalla et al. 2002). For mass balance calculations we chose an averaged value of $^{fluid/melt}D_{Cl}$=10, similar to what was found by Signorelli and Carroll (2000) and Métrich et al. (2001), from which by using the average Cl concentration in CAL 1 glass we

obtain a $^{fluid}C_{Cl}$ of 1.9, representing the Cl concentration (mol%) in the fluid phase. As the Cl-enrichment should exclusively be induced by Cl in the fluid phase, we obtain the following relation:

$$\text{Fluid}_{\text{mol}} = \left(\Delta\text{Cl}_{\text{tot}} / {}^{\text{fluid}}C_{\text{Cl}}\right) \times 100 = 1.0 \times 10^{12}\text{moles}$$

which can be assumed as the amount of volatiles needed to differentiate 6.1×10^{13} moles of magma emitted in the last phase of the Laghetto eruption, resulting in a fluid/melt molar ratio of ~1:7.

References

Allard P (1997) Endogenous magma degassing and storage at Mount Etna. Geophys Res Lett 24(17):2219–2222

Allard P, Carbonelle J, Dajlevic D, Le Bronec J, Morel P, Robe MC, Maurenas JM, Faivre-Pierret R, Martin D, Sabroux JC, Zettwoog P (1991) Eruptive and diffuse emissions of CO_2 from Mount Etna. Nature 351:387–391

Alletti M, Aiuppa A, Baker DR, Freda C (2006) Fluid/melt partitioning coefficients of chlorine in basaltic melt. Geophys Res Abstr 8:08823

Alparone S, Andronico D, Giammanco S, Lodato L (2004) A multidisciplinary approach to detect active pathways for magma migration and eruption at Mt. Etna (Sicily, Italy) before the 2001 and 2002–2003 eruptions. J Volcanol Geotherm Res 136:121–140

Armienti P, Innocenti F, Petrini R, Pompilio M, Villari L (1989) Petrology and Sr-Nd isotope geochemistry of recent lavas from Mt. Etna: bearing on the volcano feeding system. J Volcanol Geotherm Res 39:315–327

Armienti P, Tonarini S, D'Orazio M, Innocenti F (2002) Genesis and evolution of Mt. Etna alkaline lavas: petrological and Sr-Nd-B isotope constraints. Period Mineral 73:29–52

Asimow PD, Ghiorso MS (1998) Algorithmic modifications extending MELTS to calculate subsolidus phase relations. Am Mineral 83:1127–1131

Bachmann O, Bergantz GW (2004) On the origin of crystal-poor rhyolites: extracted from batholithic crystal mushes. J Petrol 45 (8):1565–1582

Barbieri M, Cristofolini R, Delitala MC, Fornaseri M, Romano R, Taddeucci A, Tolomeo L (1993) Geochemical and Sr-isotope data on historic lavas of Mount Etna. J Volcanol Geotherm Res 56(1–2):57–69

Beermann O, Stelling J, Nowak M, Botcharnikov RE (2006) Partitioning of chlorine between H_2O-bearing fluid and basaltic melt on Mount Etna. XXVII (14) Arbeitstagung, Modellierungen von Strukturen und Strukturbildungsprozessen in nichkristallinen Materialien, 28–30 August, Wolfersdorf

Behncke B, Neri M (2003) The July–August 2001 eruption of Mt. Etna (Sicily). Bull Volcanol 65:461–476

Bhalla P, Blaine F, Holtz F, Brugmann G, Wittenberg A, Nowak M (2002) Chloride distribution between hydrous fluid and basalt at 0.1–0.2 GPa; effect of chloride on Pt solubility. J Conf Abs EMPG IX:12

Billi A, Acocella V, Funiciello R, Giordano G, Lanzafame G, Neri M (2003) Mechanism for ground-surface fracturing and incipient slope failure associated with the 2001 eruption of Mt. Etna, Italy: analysis of ephemeral field data. J Volcanol Geotherm Res 22:281–294

Bohrson WA, Reid MR (1997) Genesis of silicic perakaline volcanic rocks in an ocean island setting by crustal melting and open-system processes: Socorro Island, Mexico. J Petrol 38:1137–1166

Bonaccorso A, Aloisi M, Mattia M (2002) Dike emplacement forerunning the Etna July 2001 eruption modelled through continuous tilt and GPS data. Geophys Res Lett 29(2):1–4

Bonaccorso A, D'Amico S, Mattia M, Patanè D (2004) Intrusive mechanism at Mt. Etna forerunning the July–August 2001 eruption. Pure Appl Geophys 161(7):1469–1487

Boudreau AE, Mathez EA, McCallum IS (1986) Halogen geochemistry of the Stillwater and Bushveld complexes: evidence for transport of the platinum group elements by Cl-rich fluids. J Petrol 27:627–645

Burnham CW (1979) Magmas and hydrothermal fluids. In: Barnes HL (ed) Geochemistry of hydrothermal ore deposits. Wiley, New York, pp 71–136

Calvari S, Pinkerton H (2004) Birth, growth and morphologic evolution of the "Laghetto" cinder cone during the 2001 Etna eruption. J Volcanol Geotherm Res 132:225–239

Caracausi A, Favara R, Giammanco S, Italiano F, Nuccio PM, Paonita A, Pecoraino G, Rizzo A (2003a) Mount Etna: geochemical signal of magma ascent and unusually extensive plumbing system. Geophys Res Lett 30:1057

Caracausi A, Italiano F, Paonita A, Rizzo A, Nuccio PM (2003b) Evidence of deep magma degassing and ascent by geochemistry of peripheral gas emissions at Mount Etna (Italy): assessment of the magmatic reservoir pressure. J Geophys Res 108:B102463, DOI 10.1029/2002JB002095

Caroff M, Ambrics C, Maury RC, Cotton J (1997) From alkali basalt to phonolite in hand-size samples: vapor-differentiated effects in the Bouzentes lava flow (Cantal, France). J Volcanol Geotherm Res 79:47–61

Carroll MR (2005) Chlorine solubility in evolved alkaline magmas. Ann Geophys 48(4–5):619–631

Clocchiatti R, Tanguy JC (2001) Amphibole megacrysts from the 2001 S-flank eruption, Etna, Italy. Bull Glob Volcanism Netw Smithson Inst 26:3–4

Clocchiatti R, Joron JL, Treuil M (1988) The role of selective alkali contamination in the evolution of recent historic lavas of Mt. Etna. J Volcanol Geotherm Res 34:241–249

Clocchiatti R, Weisz J, Mosbah M, Tanguy JC (1992) Coexistence of CO_2-saturated alkaline and tholeiitic "glasses" within the olivines of the Aci Castello hyaloclastites (Etna, Sicily, Italy). Issues supporting an anomalous mantle and a deep reservoir (In French). Acta Vulcanol 2:161–173

Clocchiatti R, Condomines M, Guènot N, Tanguy JC (2004) Magma changes at Mount Etna: the 2001 and 2002–2003 eruptions. Earth Planet Sci Lett 226:397–414

Condomines M, Tanguy JC, Michaud V (1995) Magma dynamics at Mt Etna: constraints from U-Th-Ra-Pb radioactive disequilibria and Sr isotopes in historical lavas. Earth Planet Sci Lett 132:25–41

Corsaro RA, Cristofolini R (1996) Origin and differentiation of recent basaltic magmas from Mount Etna. Mineral Petrol 57:1–21

Corsaro RA, Miraglia L (2005) Dynamics of 2004–2005 Mt. Etna effusive eruption as inferred from petrologic monitoring. Geophys Res Lett 32:L13302, DOI 10.1029/2005GL022347

Corsaro RA, Miraglia L, Pompilio M. (2007) Petrologic evidence of a complex plumbing system feeding the July–August 2001 eruption of Mt. Etna, Sicily, Italy. Bull Volcanol 69:401–421, DOI 10.1007/s00445-006-0083-4

Cristofolini R, Romano R (1982) Petrological features of Etnean volcanic rocks. Mem Soc Geol Ital 23:99–115

Cristofolini R, Albini A, Di Girolamo P, Stanzione D (1981) Geochemistry of some volcanic rocks from South-eastern Sicily: rare earth and other trace element distribution. Bull Volcanol 44:95–107

Davies GR, MacDonald R (1987) Crustal influences in the petrogenesis of the Naivasha basalt-comendite complex: combined trace element and Sr-Nd-Pb isotope constraints. J Petrol 28:1009–1031

De Hoogh JCM, Van Bergen MJ (2000) Volatile-induced transport of HFSE, REE, Th and U in arc magmas: evidence from zirconolite-bearing vesicles in potassic lavas of Lewotolo volcano (Indonesia). Contrib Mineral Petrol 139:485–502

Ferlito C, Siewert J (2006) Lava channel formation during the 2001 eruption on Mount Etna: evidence for mechanical erosion. Phys Rev Lett 96:028501

Gardner JE, Burgisser A, Hort M, Rutherford M (2006) Experimental and model constraints on degassing of magma during ascent and eruption. In: Siebe C, Macias JL, Aguirre-Diaz GJ (eds), Neogene-quaternary continental margin volcanism: a perspective from Mexico, Geol. Soc. Amer. Spec. Paper 402, Penrose Conf. Series, pp 99–113, DOI 10.1130/2006.2402(04)

Ghiorso MS, Sack RO (1995) Chemical mass transfer in magmatic processes 4. A revised and internally consistent thermodynamic model for the interpolation and extrapolation of liquid-solid equilibria in magmatic systems at elevated temperatures and pressures. Contrib Mineral Petrol 119:197–212

Greenough JD, Lee CY, Fryer BJ (1999) Evidence for volatile-influenced differentiation in a layered alkali basalt flow, Penghu Island, Taiwan. Bull Volcanol 60:412–424

Hedenquist JW, Lowenstern JB (1994) The role of magmas in the formation of hydrothermal ore deposits. Nature 370:519–527

Jarosewich E, Nelen JA, Norberg JA (1980) Reference samples for electron microprobe analysis. Geostand Newsl 4(1):43–47

Joron JL, Treuil M (1984) Geochemical and petrogenetic study of Etna lavas, Sicily (Italy) (In French). Bull Volcanol 47:1125–1144

Kamenetsky V, Clocchiatti R (1996) Primitive magmatism of Mt. Etna: insights from mineralogy and melt inclusions. Earth Planet Sci Lett 142:553–572

Keppler H, Wyllie PJ (1990) Role of fluids in transport of uranium and thorium in magmatic processes. Nature 348:531–533

Keppler H, Wyllie PJ (1991) Partitioning of Cu, Sn, Mo, W, U, and Th between melt and aqueous fluid in the system haplogranite-H_2O-HCl and haplogranite-H_2O-HF. Contrib Mineral Petrol 109:139–150

Kodosky LG, Keith TEC (1993) Factors controlling the geochemical evolution of fumarolic encrustations, Valley of Ten Thousand Smokes, Alaska. J Volcanol Geotherm Res 55:185–200

Lanzafame G, Neri M, Acocella V, Billi A, Funiciello R, Giordano G (2003) Structural features of the July-August 2001 Mount Etna eruption evidence for a complex magma supply system. J Geol Soc (Lond) 160:531–544

Lautze NC, Harris AJL, Bailey JE, Ripepe M, Calvari S, Dehn J, Rowland SK, Jones KE (2004) Pulsed lava effusion at Mount Etna during 2001. J Volcanol Geotherm Res 137:231–246

Le Guern F, Bernard A (1982) Study of condensation mechanisms of magmatic gases. The Etna (Italy) example (In French). Bull Volcanol 45:161–166

Le Guern F, Shinohara H (1985) Etna 1983 composition of the magmatic gases. Abstract for IAVCEI 1985 scientific assembly

Le Maitre RW (2002) A classification of igneous rocks and glossary of terms. Cambridge University Press, Cabridge, UK, pp 1–236

MacDonald R, Upton BGJ, Thomas JE (1973) Potassium- and fluorine-rich hydrous phase coexisting with peralkaline granite in South Greenland. Earth Planet Sci Lett 18:217–222

MacDonald R, Davies GR, Bliss CM, Leat PT, Bailey DK, Smith RL (1987) Geochemistry of high-silica peralkaline rhyolites, Naivasha, Kenya Rift Valley. J Petrol 28:979–1008

Métrich N, Rutherford MJ (1992) Experimental study of chlorine behavior in hydrous silicic melts. Geochim Cosmochim Acta 56:607–616

Métrich N, Rutherford MJ (1998) Low pressure crystallization paths of H_2O-saturated basaltic-hawaiitic melts from Mt. Etna: implications from open-system degassing of basaltic volcanoes. Geochim Cosmochim Acta 62(7):1195–1205

Métrich N, Bertagnini A, Landi P, Rosi M (2001) Crystallization driven by decompression and water loss at Stromboli volcano (Aeolian Islands, Italy). J Petrol 42(8):1471–1490

Métrich N, Allard P, Spilliaert N, Andronico D, Burton M (2004) 2001 flank eruption of the alkali- and volatile-rich primitive basalt responsible for Mount Etna's evolution in the last three decades. Earth Planet Sci Lett 228:1–17

Monaco C, Catalano S, Cocina O, De Guidi G, Ferlito C, Gresta S, Musumeci C, Tortorici L (2005) Tectonic control on the eruptive dynamics at Mt. Etna Volcano (Sicily) during the 2001 and 2002–2003 eruptions. J Volcanol Geotherm Res 144:211–233

Newman S, Lowenstern JB (2002) VOLATILECALC: a silicate melt-H_2O-CO_2 solution model written in Visual Basic Excel. Comput Geosci 2:597–604

Patanè D, Chiarabba C, Cocina O, De Gori P, Moretti M, Boschi E (2002) Tomographic images and 3D earthquake locations of the seismic swarm preceding the 2001 Mt. Etna eruption: evidence for a dyke intrusion. Geophys Res Lett 29(135):1–4

Rae DA, Coulson IM, Chambers AD (1996) Metasomatism in the North Qoroq centre, South Greenland: apatite chemistry and rare-earth element transport. Mineral Mag 60:207–220

Rittmann A (1962) Volcanoes and their activity. Wiley, New York, 305 pp

Salvi S, William-Jones AE (1996) The role of hydrothermal processes in concentrating high-field strength elements in the Strange Lake peralkaline complex, north-eastern Canada. Geochim Cosmochim Acta 60:1917–1932

Schiano P, Clocchiatti R, Ottolini L, Busà T (2001) Transition of Mount Etna lavas from a mantle-plume to an island-arc magmatic source. Nature 412:900–904

Shinohara H, Iiyama JT, Matsuo S (1989) Partition of chlorine compounds between silicate melt and hydrothermal solutions. Geochim Cosmochim Acta 53:2617–2630

Signorelli S, Carroll MR (2000) Solubility and fluid-melt partitioning of Cl in hydrous phonolitic melts. Geochim Cosmochim Acta 64:2851–2862

Spilliaert N, Métrich N, Allard P (2006) S-Cl-F degassing pattern of water-rich alkali basalt: modelling and relationship with eruption styles on Mount Etna volcano. Earth Planet Sci Lett 248:772–786

Stormer JC, Nicholls J (1978) XLFRAC a program for interactive testing of magmatic differentiation models. Comput Geosci 4:143–159

Symonds RB, Rose WI, Bluth GJS, Gerlach TM (1994) Volcanic-gas studies: methods, results and applications. In: Carrol MR, Holloway JR (ed) Volatiles in magmas. Rev Miner 30:1–66

Taddeucci J, Pompilio M, Scarlato P (2002) Monitoring the explosive activity of the July–August 2001 eruption of Mt. Etna (Italy) by ash characterization. Geophys Res Lett 29(8) DOI 10.1029/2001GL014372

Taddeucci J, Pompilio M, Scarlato P (2004) Conduit processes during the July-August 2001 explosive activity of Mount Etna (Italy): inferences from glass chemistry and crystal size distribution of ash particles. J Volcanol Geotherm Res 137:33–54

Tanguy JC, Condomines M, Kieffer G (1997) Evolution of Mount Etna magma: constraints on the present feeding system and eruptive mechanism. J Volcanol Geotherm Res 75:221–250

Taylor RP, Strong DF, Fryer BJ (1981) Volatile control of contrasting trace element distributions in peralkaline granitic and volcanic rocks. Contrib Mineral Petrol 77:267–271

Tonarini S, Armienti P, D'Orazio M, Innocenti F, Pompilio M, Petrini R (1995) Geochemical and isotopic monitoring of Mt. Etna

1989–1993 eruptive activity: bearing on the shallow feeling system. J Volcanol Geotherm Res 64:95–115

Tonarini S, Armienti P, D'Orazio M, Innocenti F (2001) Subduction-like fluids in the genesis of Mt. Etna magmas: evidence from boron isotopes and fluid mobile elements. Earth Planet Sci Lett 192:471–483

Viccaro M (2006) Genesis, differentiation and eruptive dynamics of Mt. Etna magmas. PhD Thesis, University of Catania (Italy)

Viccaro M, Ferlito C, Cortesogno L, Cristofolini R, Gaggero L (2006) Magma mixing during the 2001 event at Mt. Etna (Italy): effects on the eruptive dynamics. J Volcanol Geotherm Res 149:139–159

Webster JD (1992) Fluid-melt interactions involving Cl-rich granites; experimental studies from 2 to 8 kbar. Geochim Cosmochim Acta 56:659–678

Webster JD (1997) Exsolution of magmatic volatile phases from Cl-enriched mineralizing granitic magmas and implications for ore metal transport. Geochim Cosmochim Acta 61:1017–1029

Webster (2004) The exsolution of magmatic hydrosaline chloride liquids. Chem Geol 210(1–4):33–48

Webster JD, De Vivo B (2002) Experimental and modeled solubilities of chlorine in aluminosilicate melts, consequences of magma evolution, and implications for exsolution of hydrous chloride melt at Mt. Somma-Vesuvius. Am Mineral 87(8–9):1046–1061

Webster JD, Kinzler RJ, Mathez EA (1999) Chloride and water solubility in basalt and andesite melts and implications for magmatic degassing. Geochim Cosmochim Acta 63(5):729–738

Wehrmann H (2005) Volatile degassing and plinian eruption dynamics of the mafic Fontana Tephra, Nicaragua. PhD Thesis, University of Kiel (Germany)

Wilkinson JJ, Nolan J, Rankin AH (1996) Silicothermal fluid: a novel medium for mass transport in the lithosphere. Geology 24:1059–1062